Fundamental, Multipole, and Half-Vortex Gap Solitons in Spin-Orbit Coupled Bose-Einstein Condensates

Valery E. Lobanov,[1] Yaroslav V. Kartashov,[1,2] and Vladimir V. Konotop[3,4]
[1]ICFO-Institut de Ciencies Fotoniques and Universitat Politecnica de Catalunya, 08860 Castelldefels (Barcelona), Spain
[2]Institute of Spectroscopy, Russian Academy of Sciences, Troitsk, Moscow Region 142190, Russia
[3]Centro de Física Teórica e Computacional, Faculdade de Ciências, Universidade de Lisboa, Avenida Professor Gama Pinto 2, Lisboa 1649-003, Portugal
[4]Departamento de Física, Faculdade de Ciências, Universidade de Lisboa, Campo Grande, Edifício C8, Lisboa 1749-016, Portugal
(Received 6 November 2013; published 7 May 2014)

Using the parity and time reversal symmetries of a two-dimensional spin-orbit coupled Bose-Einstein condensate in a lattice created by the Zeeman field, we identify and find numerically various families of localized solutions, including multipole and half-vortex solitons. The obtained solutions may exist at any direction of the gauge field with respect to the lattice and can be found either in finite gaps (for repulsive interatomic interactions) or in a semi-infinite gap (for attractive interactions). The existence of half-vortices requires higher symmetry (the reflection with respect to the field direction). Stability of these modes makes them feasible for experimental observation.

DOI: 10.1103/PhysRevLett.112.180403 PACS numbers: 03.75.Lm, 03.75.Mn, 71.70.Ej

A spin-orbit coupled Bose-Einstein condensate (SO-BEC) [1] is a model where a synthetic spin degree of freedom coupled with the momentum allows one to simulate spin-orbit interactions in solid state systems and at the same time naturally introduces different types of gauge fields [2] which can be created and controlled by external laser beams. The SO-BEC has acquired particular importance after it was realized experimentally [3].

One can mention several distinguishing properties of SO-BECs. First, due to linear coupling the atomic spectrum is characterized by degeneracy of the energy minima at finite momenta. This gives origin to stripe phases in two-dimensional [4–6] and in one-dimensional [7] geometries. Another inherent feature is the nonlinearity, stemming from interatomic interactions, which in one-dimensional case may lead to formation of vector stripe-solitons [8–10]. Finally, due to the spinor nature a SO-BEC supports topological modes termed half-vortices. Such modes can be characterized by 2π rotation of the phase of one of the component on the closed contour surrounding the mode center and zero change of the total phase of the second component. Half-vortices exist in ^{3}He [11], and recently they were predicted [12] and observed [13] in exciton-polariton condensates. Considerable attention was paid to vortical structures in repulsive SO-BEC in a parabolic trap [6,14,15] and vortex lattices were obtained in the presence of optical lattice [16].

Turning to SO-BEC in a periodic environment, a lattice can be created in different ways: as a periodic trapping potentials for each of spinor components [16–18], by spatially modulating Raman coupling [19], or by imposing spatially dependent (periodic) Zeeman field [10,20–22]. In the latter case the lattice appears exactly "inverted" for the condensate components. One-dimensional solitons in such lattices were addressed only recently in [10].

So far, however, no spatially localized matter-wave solitons were reported in a two-dimensional SO-BEC in lattice potentials. Meanwhile, two-dimensional lattices may support solitons with nontrivial topologies, such as vortical states, which do not exist in the one-dimensional geometry. Due to the specific "inverted" character of Zeeman lattice (ZL) for the spinor components the existence and stability of two-dimensional solitons require separate analysis, especially for attractive interactions. In this Letter, for the first time, we show that a rich variety of two-dimensional stable solitons may exist in SO-BEC held in a Zeeman lattice. Such solutions can be obtained and classified on the basis of symmetries imposed by the ZL.

A SO-BEC obeys an intrinsic anisotropy introduced by the gauge field which in the absence of a lattice determines the mirror-reflection symmetry. The degeneracy of the linear spectrum imposes an additional spatial scale (defined by the Bloch vectors of the degenerate points). External periodic potentials may break the mirror symmetry and introduce additional spatial scales. Thus, the interplay between gauge field and lattice, which in the two-dimensional case can have different orientations, may affect in a nontrivial way the existence, structure, and stability of nonlinear excitations. Two-dimensional solitons and their relation with symmetries of a SO-BEC constitute the main issue of this Letter.

We consider a SO-BEC described by the spinor $\Psi = \mathrm{col}(\Psi_1, \Psi_2)$ in a two-dimensional square ZL $\Omega(\mathbf{r}) = \Omega(\mathbf{r}+\mathbf{e}_1) = \Omega(\mathbf{r}+\mathbf{e}_2)$, where $\mathbf{e}_{1,2}$ are the lattice vectors satisfying $\mathbf{e}_1\mathbf{e}_2 = 0$ and $|\mathbf{e}_{1,2}| = d$ with d being the lattice constant (see the Supplemental Material [23]). We assumed

that in the transverse direction the condensate is confined by a strong harmonic trap (of the frequency ω_0) and the recoil energy $E_r = 4\pi^2\hbar^2/(md^2)$ (m being the atomic mass) is small compared to $\hbar\omega_0$. Letting the weights γ of the Rashba [24] and Dresselhaus [25] couplings to be equal, the system Hamiltonian can be written as $H = H_{\rm lin} + H_{\rm nl}$, whose linear part is given by [10,20,26] $H_{\rm lin} = \mathbf{p}^2/(2m) - \hbar\gamma\sigma_1 p_x - \hbar\Omega(\mathbf{r})\sigma_3/2$ ($\sigma_{1,2,3}$ are the Pauli matrices). The nonlinear coupling occurs due to two-body interactions: $H_{\rm nl} = g\Psi^\dagger\Psi$, where inter- and intraspecies interaction strengths are assumed to be equal to g (e.g., for $F = 1$ and $F = 2$ states of ^{87}Rb atoms the scattering lengths differ by a few percents [3,27]). For generality of results, we consider both positive and negative scattering lengths.

We are interested in spatially localized stationary solutions $\Psi = \psi(\mathbf{r})e^{-i\mu t/\hbar}$, where $\psi(\mathbf{r})$ solves the stationary coupled Gross-Pitaevskii (GP) equations and μ is the chemical potential. Choosing the coordinate axes along $\mathbf{e}_{1,2}$, we introduce the two-dimensional gauge field $\mathbf{A} = -\gamma\sigma_1\mathbf{e}$, where $\mathbf{e} = (\cos\varphi, \sin\varphi)$ and $\varphi \in [0, \pi/4]$. Then the GP equations read

$$\mu\psi = -\frac{1}{2}\nabla^2\psi + i\mathbf{A}\nabla\psi - \frac{\sigma_3}{2}\Omega(\mathbf{r})\psi + g(\psi^\dagger\psi)\psi, \quad (1)$$

where $\mathbf{r} = (\eta, \zeta)$, $\nabla = (\partial_\eta, \partial_\zeta)$, and we adopted the dimensionless units in which spatial scales are normalized to d, the energy is measured in E_r units and $g = 1$ ($g = -1$) stands for positive (negative) scattering length. Then, for ^{87}Rb atoms (the scattering length $\sim$5.29 nm) confined by the harmonic trap with $\omega_0 = 140$ Hz the real number of atoms is $\approx 110 \times N$, where $N = N_1 + N_2$ and $N_j = \int |\psi_j|^2 d\mathbf{r}$ are computed in the dimensionless units.

We explore a separable potential, $\Omega(\mathbf{r}) = \delta\{\cos[2(\eta - \eta_0)] + \cos[2(\zeta - \zeta_0)]\}$, not fixing yet the origin of the coordinates, i.e., $\mathbf{r}_0 = (\eta_0, \zeta_0)$. Below we set $\delta = 6$. The band-gap structure of the ZL is shown in Fig. 1 (left panel). At $\gamma = 0$ the spinor components obey equivalent spectra, determining the degenerate spectrum of the total system. The SO coupling strongly modifies the band edges lifting the degeneracy of the bands, which coincide at $\gamma = 0$, transforming them into two intersecting surfaces. The first finite gap (located initially between two pairs of degenerate bands) gradually shrinks with γ and ceases to exist at $\gamma = \gamma_{\rm max}$ [the vertical dashed line in Fig. 1 (right panel)]. Thus SO coupling qualitatively affects the linear spectrum, thereby affecting domains of soliton existence because the chemical potential of solitons must fall into one of the spectrum gaps. Our consideration is restricted to the semi-infinite and the first finite gaps, i.e., to $0 < \gamma < \gamma_{\rm max}$.

To find fundamental symmetries of the system in the presence of both the field $\mathbf{A}$ and ZL, we introduce parity (P) and time (T) reversal operators acting as $Pf(\mathbf{r}, t) = f(-\mathbf{r}, t)$ and $Tf(\mathbf{r}, t) = f^*(-\mathbf{r}, t)$. We also consider an operator $\hat{a}$, such that if ψ is a solution of (1), then $\hat{a}\psi$ is also

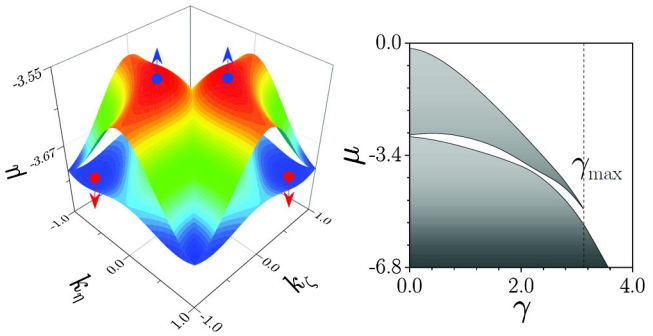

FIG. 1 (color online). Left panel: The first and second bands of the ZL spectrum vs Bloch momentum $\mathbf{k} = (k_\eta, k_\zeta)$ at $\gamma = 2$. Lower red (upper blue) arrows indicate the points from which solitons bifurcate in the case of attractive (repulsive) interactions. Right panel: Edges of semi-infinite and first finite gaps vs SO coupling strength. Gaps are shaded, while bands are shown white. In all cases $\delta = 6$, $\varphi = \pi/4$. At $\gamma = 0$ the band between semi-infinite and first finite gaps is narrow but nonzero: $\delta\mu \approx 0.049$.

the solution, generally speaking different from ψ, and identify an $\hat{a}$-symmetric solution $\psi(\mathbf{r})$ as a solution satisfying $\psi(\mathbf{r}) = \hat{a}\psi(\mathbf{r})$. Limiting the consideration to the lowest symmetries, $\hat{a}^2 = 1$, any branch of $\hat{a}$-symmetric nonlinear modes bifurcating from a linear Bloch state [28] is found as $\psi_{\mathbf{k}} + \hat{a}\psi_{\mathbf{k}}$ where $\psi_{\mathbf{k}}$ is a linear Bloch state.

Presence of the SO coupling imposes important constraints on the symmetries of the system. One of the symmetry operators is readily found: $\hat{a}_3 = \sigma_3 T$. An $\hat{a}_3$-symmetric solution can be written as $\mathrm{col}(\phi_1(\mathbf{r}), i\phi_2(\mathbf{r}))$, where $\phi_{1,2}$ are real functions (see the Supplemental Material [23]). To find other symmetries we distinguish high-symmetry points of the lattice which can be grouped as symmetric, $P\Omega = \Omega$, or antisymmetric, $P\Omega = -\Omega$, with respect to the parity transformation around these points (we call them α and β points). We consider modes localized around $\mathbf{r} = 0$ and select the following positions of the lattice: $\mathbf{r}_0 = (0, 0)$ for α points and $\mathbf{r}_0 = (\pm\pi/4, \pm\pi/4)$ for β points.

Starting with attractive interactions and α points we find that in addition to the symmetry $\hat{\alpha}_3 = \hat{a}_3$ [the symmetry operators for α (β) points are designated as $\hat{\alpha}$ ($\hat{\beta}$); $\hat{1}$ is the identity operator], we find the symmetry transformations $\hat{\alpha}_1 = \sigma_3 P$ and $\hat{\alpha}_2 = PT$ and verify that $\{\hat{1}, \hat{\alpha}_1, \hat{\alpha}_2, \hat{\alpha}_3\}$ constitute a Klein four-group (or Vierergruppe) that is characterized by the relations $\hat{\alpha}_i\hat{\alpha}_j = \hat{\alpha}_j\hat{\alpha}_i = \hat{\alpha}_k$ (for all indexes different). This group property has an interesting consequence: if a solution obeys more than one symmetry, it obeys all the symmetries of the group; i.e., a solution is either symmetric for a given j: $\psi = \hat{\alpha}_j\psi$, or highly symmetric satisfying $\psi = \hat{\alpha}_1\psi = \hat{\alpha}_2\psi = \hat{\alpha}_3\psi$. Such highly symmetric solutions obtained numerically from (1) for μ falling to semi-infinite gap are shown in Figs. 2(a), 3(a), 3(c).

Further, we separate the atomic density $n_j(\mathbf{r})$ and phase $\theta_j(\mathbf{r})$ of the jth component: $\psi_j = [n_j(\mathbf{r})]^{1/2}e^{i\theta_j(\mathbf{r})}$. In these terms for $\hat{\alpha}_1$-symmetric solutions $\theta_1(\mathbf{r}) = \theta_1(-\mathbf{r})$ and

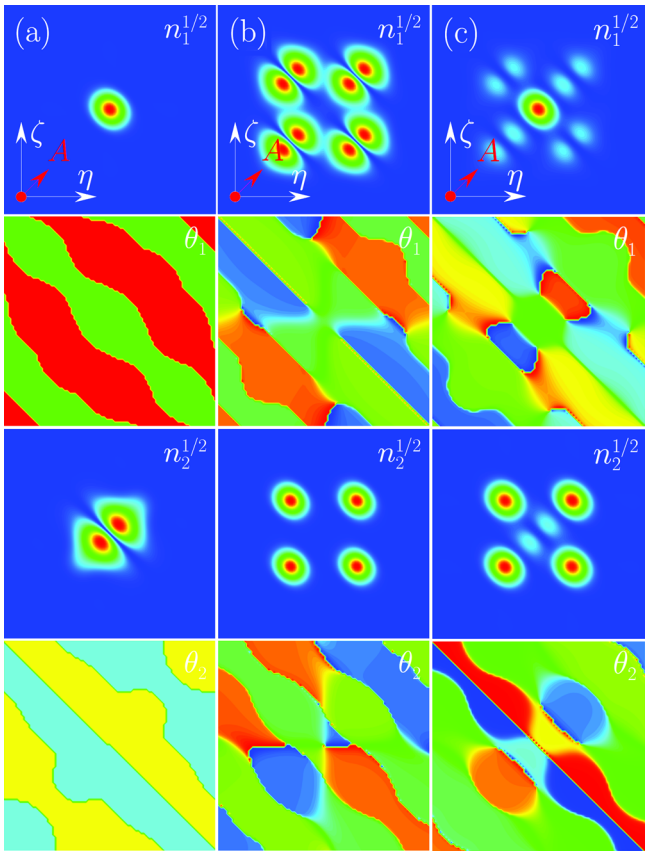

FIG. 2 (color online). Spinor amplitudes and phases in the attractive case for $\gamma = 2$. For (a) highly symmetric fundamental soliton with $\mu = -4.2$ (stable almost in the entire existence domain), (b) $\hat{\alpha}_1$-symmetric half-vortex soliton with $\mu = -5$ (stable for $\mu < -4.74$), and (c) $\hat{\alpha}_2$-symmetric soliton-quadrupole structure with $\mu = -5$ (stable for the given chemical potential). The gauge field direction is indicated in the upper panels.

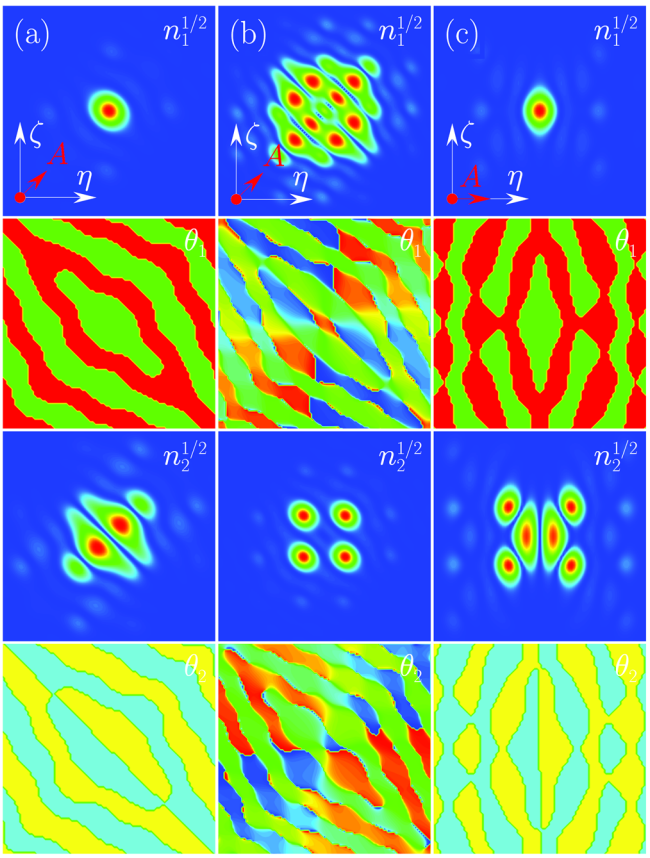

FIG. 3 (color online). Amplitudes and phases in the repulsive case for $\gamma = 2$ and $\mu = -3$ for (a) highly symmetric mode in a gap (stable almost in the entire existence domain); (b) unstable $\hat{\alpha}_2$-symmetric half-vortex soliton; and (c) highly symmetric soliton (stable for a given chemical potential).

$\theta_2(\mathbf{r}) = \theta_2(-\mathbf{r}) + \pi$. Thus, at $\mathbf{r} = 0$ the phase of the second component has either a singularity or a jump, while its density vanishes at $\mathbf{r} = 0$; i.e., such a component must have vortical or multipole structure. If the first component does not carry central phase singularity, while second component carries it, one obtains a half-vortex soliton [Fig. 2(b)]. Multipole structure of second component can be observed in simplest fundamental soliton in Fig. 2(a). $\hat{\alpha}_2$-symmetric solutions have antisymmetric phases: $\theta_{1,2}(\mathbf{r}) = -\theta_{1,2}(\mathbf{r})$. Such modes can not carry vorticity. By definition $\hat{\alpha}_2$-symmetric modes are PT symmetric. An example of such a mode found from Eq. (1) at $g < 0$ is shown in Fig. 2(c).

For repulsive interactions the modes centered in α points can be found in the first finite gap (Fig. 3). The bifurcation now occurs from maxima of $\mu(\mathbf{k})$ surface as shown by blue arrows in the left panel of Fig. 1. In two-dimensional geometry fundamental solitons always bifurcate from the internal points of the Brillouin zone (see Fig. 1); i.e., they all feature stripelike structure that is most clearly visible from stripe-phase distributions in Figs. 2 and 3. In particular, in Fig. 3(a) and 3(c) the phases $\theta_{1,2}$ take one of the values, 0 or π (θ_1) and $\pm\pi/2$ (θ_2), which is consistent with $\hat{\alpha}_3$ symmetry.

The properties of fundamental and half-vortex solitons in ZL are summarized in Fig. 4. From the panels (a) and (b) we observe that while the numbers of atoms grow almost everywhere as the branches go outwards the gap edges (the allowed band corresponds to $-3.56 < \mu < -2.75$), the magnetization $M = (N_1 - N_2)/N$ starting with zero value at the edges rapidly achieves saturation meaning that the relative populations of the components are weakly dependent on N. In the case of fundamental soliton the number of atoms in the first component always exceeds the number of atoms in the second component [$M > 0$ in Fig. 4(a)]. In the case of half-vortex solution we observe opposite relation: $N_2 > N_1$ [$M < 0$ in Fig. 4(b)]. While simplest fundamental solitons are stable almost in the entire existence domain, stable half-vortex solitons were found only for attractive interactions below certain critical value of chemical potential. In Fig. 4(c) we show the dependence of the number of atoms in the spinor components on the coupling constant for repulsive interactions: at fixed μ localized modes can be

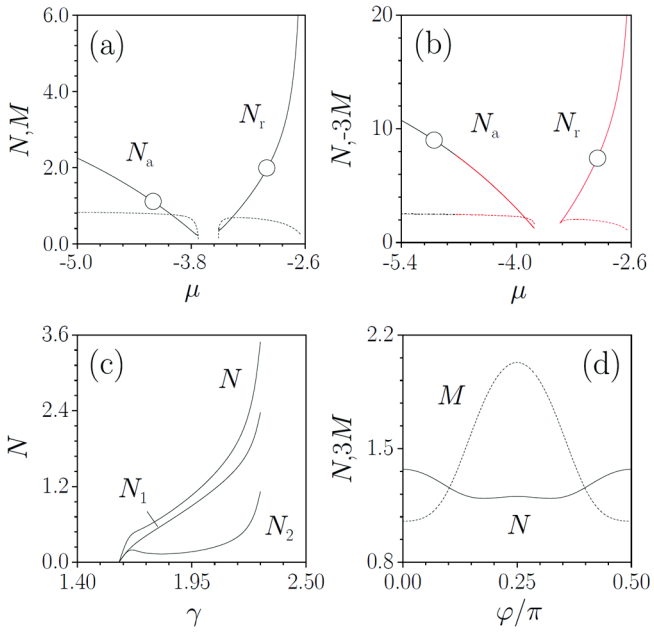

FIG. 4 (color online). Number of particles (solid curves) and magnetization (dashed curves) vs μ for fundamental (a) and half-vortex (b) solitons at $\gamma = 2$, $\varphi = \pi/4$ in attractive (subscripts a) and repulsive (subscripts r) condensates. Circles in (a) [(b)] correspond to solitons shown in Figs. 2(a) [2(b)] and 3(a) [3(b)]. Black (red) lines show stable (unstable) families. (c) $N(\gamma)$ at $\varphi = \pi/4$, and (d) N and M vs φ at $\gamma = 2$ for fundamental solitons in a repulsive SO-BEC. In (c),(d) $\mu = -3.2$.

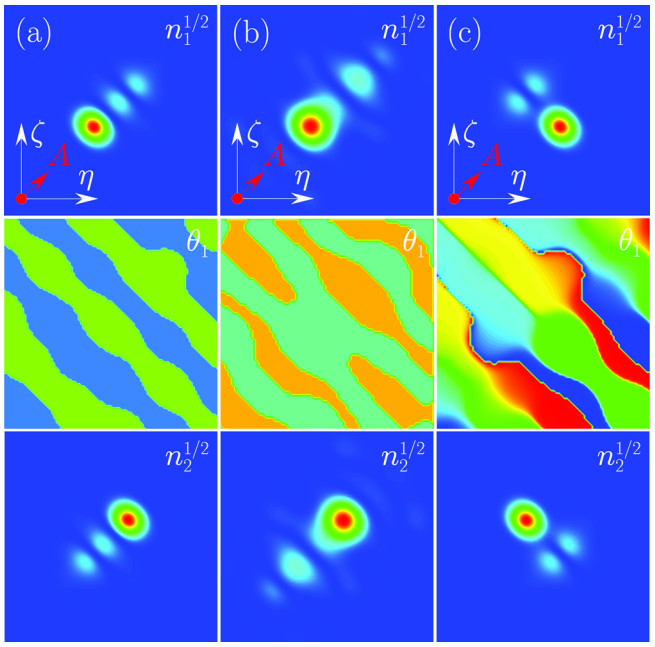

FIG. 5 (color online). Amplitudes and phases of fundamental $\hat{\beta}_1$-symmetric solitons for (a) $\mu = -4.2$ and $g = -1$; (b) $\mu = -3$ and $g = 1$; (c) $\mu = -4.2$ and $g = 1$. In all cases $\gamma = 2$. In (a) and (b) the distributions were centered at $\eta_0 = \zeta_0 = -\pi/4$, while in (c) the center is at $\eta_0 = \pi/4$, $\zeta_0 = -\pi/4$. In (a) the soliton is stable and the phases are either $-3\pi/4$ or $\pi/4$ (the first component) and $-\pi/4$ or $3\pi/4$ (the second component). In (b) the phases are either $-3\pi/8$ or $5\pi/8$ (the first component) and $-7\pi/4$ or $\pi/8$ (the second component).

found only in a limited interval of coupling constants. The imbalance of populations in components is most pronounced near the upper edge of this interval.

While the modes (a) and (b) in Fig. 3 were obtained for the gauge field directed along the lattice diagonal ($\varphi = \pi/4$) and preserving the reflection symmetry $\eta \leftrightarrow \zeta$, the gap soliton in Fig. 3(c) exists in the gauge field along η-axis, which preserves the symmetry $\eta \leftrightarrow -\eta$. Moreover, fundamental solitons can be obtained for any φ in contrast to half-vortex solitons [Figs. 2(b) and 3(b)] which were found only at $\varphi = \pi/4$. When φ decreases from $\pi/4$ to 0, fundamental modes in both attractive and repulsive SO-BECs exhibit continuous shape transformations, that is confirmed by smooth dependence of the number of atoms and magnetization on the field direction [Fig. 4(d)]. An unexpected result is the weak dependence of the number of atoms in the fundamental soliton on the field direction vs more pronounced variations of the magnetization achieving maximum at $\varphi = \pi/4$.

Turning to β points, in addition to $\hat{\beta}_3 = \hat{a}_3$ symmetry one finds other two symmetries: $\hat{\beta}_1 = i\sigma_1 PT$ and $\hat{\beta}_2 = \sigma_2 P$; $\{\hat{1}, \hat{\beta}_1, \hat{\beta}_2, \hat{\beta}_3\}$ constitute a Klein four-group. Since now the coordinate system is centered in the points with the largest slope of the potential one expects to find solutions with spatially separated global density maxima in the components, each located in the maximum of its own lattice.

Under the parity and time symmetry transformations, such solitons require the inversion of the components, i.e., change of the internal degree of freedom (charge), and thus can be characterized as CPT symmetric. The respective CPT symmetries are provided by the $\hat{\beta}_1$ and $\hat{\beta}_2$ operators. Examples of such stable solitons are shown in Fig. 5 [since the component phases of $\hat{\beta}_j$-symmetric modes with $j = 1, 2$ are uniquely related to each other (see the Supplemental Material [23]), $\varphi_1(\mathbf{r}) = (-1)^j[\varphi_2(-\mathbf{r}) - \pi/2]$, we show only the phase of the first component]. They were found in a semi-infinite [panels (a)] and first finite gaps [panels (b)] in attractive and repulsive SO-BECs, respectively.

All solitons considered so far were centered in the lattice points symmetric with respect to the reflection symmetry. Meantime the spinor solitons can be also found with centers in the points with respect to which the lattice potential is antisymmetric, i.e., $\Omega \to -\Omega$ under the reflection $\eta \leftrightarrow \zeta$. In Fig. 5(c) we show an example of a stable $\hat{\beta}_1$-symmetric soliton centered in such a lattice point.

We conclude with two remarks. First, the $\hat{\beta}_{1,2}$ symmetries, involving the pseudo-spin inversion, are broken when the inter- and intraspecies interactions are not exactly equal. However even in this case the above classification of the modes remains valid. This stems from the structural stability of the modes with respect to variation of the

inter- and intraspecies interactions (see the Supplemental Material [23]). Even when symmetries $\hat{\beta}_{1,2}$ are broken one can classify solution as branching out from the exactly $\hat{\beta}_{1,2}$-symmetric one, obtained for all interactions equal. Second, the reported modes can be excited dynamically starting with Gaussian distributions in only one of spinor components, which can be prepared using external parabolic trap. Removal of the trap and switching on Zeeman lattice lead to temporal evolution, where spinor solitons emerge spontaneously after some transient stage whose duration is determined by the recoil energy [23].

V. V. K. acknowledges useful comments of Professor Jianke Yang. V. V. K. was supported by FCT (Portugal) Grant No. PEst-OE/FIS/UI0618/2011.

[1] T. D. Stanescu, B. Anderson, and V. Galitski, Phys. Rev. A, **78**, 023616 (2008).
[2] V. Galitski and I. B. Spielman, Nature (London) **494**, 49 (2013).
[3] Y. J. Lin, K. Jimenez-Garcia, and I. B. Spielman, Nature (London) **471**, 83 (2011).
[4] C. Wang, C. Gao, C. M. Jian, and H. Zhai, Phys. Rev. Lett. **105**, 160403 (2010).
[5] T. L. Ho and S. Zhang, Phys. Rev. Lett. **107**, 150403 (2011).
[6] S. Sinha, R. Nath, and L. Santos, Phys. Rev. Lett. **107**, 270401 (2011).
[7] D. A. Zezyulin, R. Driben, V. V Konotop, and B. A. Malomed, Phys. Rev. A **88**, 013607 (2013).
[8] V. Achilleos, D. J. Frantzeskakis, P. G. Kevrekidis, and D. E. Pelinovsky, Phys. Rev. Lett. **110**, 264101 (2013).
[9] Y. Xu, Y. Zhang, and B. Wu, Phys. Rev. A **87**, 013614 (2013).
[10] Y. V. Kartashov, V. V. Konotop, and F. Kh. Abdullaev, Phys. Rev. Lett. **111**, 060402 (2013).
[11] G. E. Volovik, *The Universe in a Helium Droplet* (Oxford University Press, New York, 2003).
[12] Y. G. Rubo, Phys. Rev. Lett. **99**, 106401 (2007).
[13] K. G. Lagoudakis, T. Ostatnický, A. V. Kavokin, Y. G. Rubo, R. André, and B. Deveaud-Plédran, Science **326**, 974 (2009).
[14] J. Radić, T. A. Sedrakyan, I. B. Spielman, and V. Galitski, Phys. Rev. A **84**, 063604 (2011).
[15] C. Wu and I. Mondragon-Shem, Chin. Phys. Lett. **28**, 097102 (2011); C.-M. Jian and H. Zhai, Phys. Rev. B, **84**, 060508 (2011); B. Ramachandhran, B. Opanchuk, X.-J. Liu, Han Pu, P. D. Drummond, and H. Hu, Phys. Rev. A **85**, 023606 (2012); C.-C. Huang and S.-K. Yip, Phys. Rev. A **88**, 013628 (2013).
[16] H. Sakaguchi and B. Li, Phys. Rev. A **87**, 015602 (2013).
[17] H. A. Cruz, V. A. Brazhnyi, V. V. Konotop, and M. Salerno, Physica (Amsterdam) **238A**, 1372 (2009).
[18] Y. Zhang and C. Zhang, Phys. Rev. A **87**, 023611 (2013).
[19] V. Ya. Demikhovskiĭ , D. V. Khomitsky, and A. A. Perov, Low Temp. Phys. **33**, 115 (2007).
[20] M. J. Edmonds, J. Otterbach, R. G. Unanyan, M. Fleischhauer, M. Titov, and P. Öhberg, New J. Phys. **14**, 073056 (2012).
[21] K. Jiménez-García, L. J. LeBlanc, R. A. Williams, M. C. Beeler, A. R. Perry, and I. B. Spielman, Phys. Rev. Lett. **108**, 225303 (2012)
[22] Y. Zhang, Li Mao, and C. Zhang, Phys. Rev. Lett. **108**, 035302 (2012).
[23] See the Supplemental Material at http://link.aps.org/supplemental/10.1103/PhysRevLett.112.180403 for a comment on the creation of the two-dimensional lattice, a table of the explored symmetry relations, and constraints they impose on the solutions. We also illustrate the structural stability of the solutions and describe a possible way of excitation of a soliton.
[24] Y. A. Bychkov and E. I. Rashba, J. Phys. C **17**, 6039 (1984).
[25] G. Dresselhaus, Phys. Rev. **100**, 580 (1955).
[26] Hui Zhai, Int. J. Mod. Phys. B **26**, 1230001 (2012).
[27] See, e.g., M. Egorov, B. Opanchuk, P. Drummond, B. V. Hall, P. Hannaford, and A. I. Sidorov, Phys. Rev. A **87**, 053614 (2013) and references therein.
[28] See, e.g., J. Wang and J. Yang, Phys. Rev. A **77**, 033834 (2008); T. Dohnal and D. Pelinovsky, Phys. Rev. E **85**, 026605 (2012).